The contractile ring coordinates curvature-dependent septum assembly during fission yeast cytokinesis

Citation: Zhou, Zhou, Emilia Laura Munteanu, Jun He, Tristan Ursell, Mark Bathe, Kerwyn Casey Huang, and Fred Chang. "The Contractile Ring Coordinates Curvature Dependent Septum Assembly During Fission Yeast Cytokinesis." Molecular Biology of the Cell (October 29, 2014).

As Published: http://dx.doi.org/10.1091/mbc.E14-10-1441

Publisher: American Society for Cell Biology

Persistent URL: http://hdl.handle.net/1721.1/92586

Version: Final published version: final published article, as it appeared in a journal, conference proceedings, or other formally published context

The contractile ring coordinates curvature-dependent septum assembly during fission yeast cytokinesis

Zhou Zhou[a], Emilia Laura Munteanu[a], Jun He[b], Tristan Ursell[c], Mark Bathe[b], Kerwyn Casey Huang[c,d], and Fred Chang[a]

[a]Department of Microbiology and Immunology, Columbia University College of Physicians and Surgeons, New York, NY 10032; [b]Department of Biological Engineering, Massachusetts Institute of Technology, Cambridge, MA 02139; [c]Department of Bioengineering, Stanford University, Stanford, CA 94305; [d]Department of Microbiology and Immunology, Stanford University School of Medicine, Stanford, CA 94305

ABSTRACT **The functions of the actin-myosin–based contractile ring in cytokinesis remain to be elucidated. Recent findings show that in the fission yeast *Schizosaccharomyces pombe*, cleavage furrow ingression is driven by polymerization of cell wall fibers outside the plasma membrane, not by the contractile ring. Here we show that one function of the ring is to spatially coordinate septum cell wall assembly. We develop an improved method for live-cell imaging of the division apparatus by orienting the rod-shaped cells vertically using microfabricated wells. We observe that the septum hole and ring are circular and centered in wild-type cells and that in the absence of a functional ring, the septum continues to ingress but in a disorganized and asymmetric manner. By manipulating the cleavage furrow into different shapes, we show that the ring promotes local septum growth in a curvature-dependent manner, allowing even a misshapen septum to grow into a more regular shape. This curvature-dependent growth suggests a model in which contractile forces of the ring shape the septum cell wall by stimulating the cell wall machinery in a mechanosensitive manner. Mechanical regulation of the cell wall assembly may have general relevance to the morphogenesis of walled cells.**

Monitoring Editor
Gero Steinberg
University of Exeter

Received: Oct 14, 2014
Accepted: Oct 24, 2014

INTRODUCTION

The contractile ring is a ubiquitous, conserved structure used for cytokinesis in animal and fungal cells. This actin-myosin–based structure has generally been believed to exert contractile force to drive the ingression of the plasma membrane at the cleavage furrow. However, recent findings have called into question the primary importance of the ring for force production in furrow ingression. In several cell types, cytokinesis has been found to proceed in the absence of myosin or myosin-motor activity, including in *Dictyostelium* (De Lozanne and Spudich, 1987), budding yeast (Bi *et al.*, 1998; Lord *et al.*, 2005; Fang *et al.*, 2010), fission yeast (Proctor *et al.*, 2012), and mammalian cells (Ma *et al.*, 2012). Thus, the functions of the contractile ring remain to be precisely defined.

Fission yeast *Schizosaccharomyces pombe* serves as a genetically tractable model for cytokinesis (Bathe and Chang, 2010; Pollard and Wu, 2010). *S. pombe* cells are rod-shaped, unicellular organisms encased in a glucan-rich cell wall that divide by medial fission. An actomyosin ring, which shares many conserved core components with the ring in animal cells (Balasubramanian *et al.*, 2004), forms just under the plasma membrane at the medial division site during mitosis. This ring is composed of short actin filaments bundled and oriented largely parallel to the plasma membrane (Kamasaki *et al.*, 2007) and contains myosin IIs, which pull on the actin filaments (Bezanilla *et al.*, 1997; Mishra *et al.*, 2013), as well as proteins that link the ring to the plasma membrane (Celton-Morizur *et al.*, 2004; Roberts-Galbraith *et al.*, 2010). At the end of mitosis, the cell wall septum begins to be formed at the site marked by the ring (Roncero and Sanchez, 2010). The septum cell wall grows inward just outside the plasma membrane, concurrent with the closure of the cytokinetic

This article was published online ahead of print in MBoC in Press (http://www.molbiolcell.org/cgi/doi/10.1091/mbc.E14-10-1441) on October 29, 2014.

Address correspondence to: Fred Chang (fc99@columbia.edu).

Abbreviations used: BFA, brefeldin A; DAPI, 4′,6-diamidino-2-phenylindole; DMSO, dimethyl sulfoxide; FITC-lectin, fluorescein isothiocyanate conjugated lectin; GFP, green fluorescent protein; LatA, latrunculin A; PDMS, polydimethylsiloxane; RFP, red fluorescent protein; Tomato, tandem tomato dimer fluorescent protein; TRITC-lectin, tetramethylrhodamine isothiocyanate-conjugated lectin.

Supplemental Material can be found at:
http://www.molbiolcell.org/content/suppl/2014/10/28/mbc.E14-10-1441v1.DC1.html

ring inside the membrane. The septum is a thin (~100-nm thickness) trilaminar structure assembled by cell wall synthases, which include Bgs1, which contributes linear β(1,3)-glucan at the primary septum (Cortes *et al.*, 2007); Bgs4, which contributes to branched β(1,3)-glucans at the secondary septum (Cortes *et al.*, 2005); and Ags1, which is responsible for α(1,3)-glucan synthesis (Cortes *et al.*, 2012).

In *S. pombe* cells, successful cytokinesis requires both the septum and ring. Mutants defective in the ring fail to form an organized septum (Nurse *et al.*, 1976; Marks *et al.*, 1987; Chang *et al.*, 1996; Gould and Simanis, 1997), suggesting that the ring is needed to template the initial location of the septum. Components of the ring may serve to recruit the septum assembly machinery to proper locations on the plasma membrane. In mutants that cannot form a septum, the ring can form but does not pinch in the membrane, instead often sliding on the plasma membrane (Jochova *et al.*, 1991; Stachowiak *et al.*, 2014). Force estimates suggest that the ring does not exert nearly enough force to work against the high turgor pressure in these cells (Proctor *et al.*, 2012; Stachowiak *et al.*, 2014). We showed that furrow ingression and septum growth can still occur in the absence of the actin ring (Proctor *et al.*, 2012). In these experiments, cells that had already initiated septation were treated with a high dose of latrunculin A (LatA) and were observed to continue furrow ingression. These findings suggest that cell wall growth pushing from outside of the membrane provides the primary force for furrow ingression in these cells. However, the slower rate of ingression in various ring mutants and in LatA-treated cells (Pelham and Chang, 2002; Lord *et al.*, 2005; Yonetani *et al.*, 2008; Sladewski *et al.*, 2009; Pollard *et al.*, 2012; Proctor *et al.*, 2012; Tebbs and Pollard, 2013) suggests that the ring may positively modulate the rate of ingression. How contractile forces exerted by the ring contribute to furrow ingression and septation is not understood.

Here we examine the function of the contractile ring for cytokinesis in fission yeast cells. We find that it mediates the spatial coordination of the assembly of the septum, so that the septum hole is round and centered. Guided by theoretical considerations (Thiyagarajan *et al.*, 2014), we find that the ring may regulate curvature-dependent cell wall growth that shapes and guides the assembly of the septum. This curvature dependence suggests that actin-myosin–dependent forces from the ring stimulate and coordinate cell wall synthesis at the septum.

RESULTS

The cytokinetic ring is required for spatial coordination of septum assembly

Because rod-shaped fission yeast cells typically lie flat relative to the coverslip, conventional approaches to imaging the entire cytokinetic ring usually involve three-dimensional (3D) reconstructions from *z*-stacks acquired perpendicular to the ring. However, spatial resolution is poor in such reconstructions, limiting the ability to determine geometric features of the division apparatus. We improved the spatial resolution by positioning fission yeast cells vertically in arrays of polydimethylsiloxane (PDMS) chambers. These circular chambers were 4 and 6 μm in diameter, which was suitable to hold *S. pombe* cells, which are ~4 μm in diameter (Figure 1A). Using this approach, we could image the ring and septum in a small number of *z*-images with much higher spatial resolution than was possible using conventional approaches. We imaged cytokinesis using 2GFP-Bgs4 to mark the septum leading edge (Cortes *et al.*, 2005, 2007) and Rlc1-tomato (myosin regulatory light chain; Le Goff *et al.*, 2000) to mark the contractile ring. In wild-type cells at 30°C, septa ingressed centripetally and usually completed cytokinesis within 20 min (Figure 1B, top). Both the septum and ring formed nearly circular patterns as they closed.

To understand the role of the actomyosin ring in this process, we inhibited F-actin polymerization by treating the cells with 200 μM LatA, which leads to the rapid, complete loss of all detectable F-actin (Chang, 1999; Pelham and Chang, 2002; Supplemental Figure S1A). The septum did not immediately change position (or pop back) upon this sudden removal of the ring, suggesting that the septum is not visibly stretched by the ring (Supplemental Figure S1B). Time-lapse images showed that the septum continued to ingress. Of interest, the septum hole became noncircular and asymmetric relative to the cell center during the progression of cytokinesis (Figure 1B, bottom). This suggests that actin is needed to maintain a round and symmetric septum hole during ingression.

Because actin affects numerous processes, we tested whether these effects on septum shape were dependent specifically on the ring. We found that conditional mutants in ring proteins *myo2-E1* (myosin heavy chain; Balasubramanian *et al.*, 1998) and *cdc12-112* (formin; Chang *et al.*, 1997) display noncircular and asymmetric septa similar to those seen in LatA-treated cells (Figure 1, C and D). Because actin also contributes to membrane trafficking, we tested whether inhibition of the secretory pathway or endocytosis causes septal shape defects. We found that in cells treated with brefeldin A (BFA; Turi *et al.*, 1994), which disrupts the Golgi apparatus, the septum ingressed more slowly but still maintained its circular shape (Supplemental Figure S1D). In an endocytosis mutant *wsp1Δ* (Lee *et al.*, 2000; Basu and Chang, 2011), the septum also ingressed with a circular hole (Supplemental Figure S1D).

To quantify these effects, we measured the "skewness," which is the distance that the septum deviated from the center of the cellular cross section, and the "circularity," which describes how round a shape is (see *Materials and Methods*). Skewness was significantly increased in LatA-treated, *myo2-E1*, and *cdc12-112* cells (p = 0.0024, 0.015, and 0.03, respectively), but not in wild-type, BFA-treated, and *wsp1Δ* cells (Figure 1F). Circularity was significantly decreased in LatA-treated, *myo2-E1*, and *cdc12-112* cells (p = 0.00021, 0.016, and 0.00043, respectively), but not in wild-type, BFA-treated, and *wsp1Δ* cells (Figure 1G). Taken together, these data show that defects in the cytokinetic ring, rather than in general membrane trafficking, are responsible for shape abnormalities of the septum. Thus the ring may function to globally coordinate septum cell wall synthesis, thereby keeping the septum hole circular and symmetric (Figure 1E).

Asymmetric septum assembly in cells with altered septum shape

If the cytokinetic ring keeps the septum hole circular, can it actively restore noncircular holes to a circular shape? We devised three ways to alter the shape of the septum. First, we slightly flattened the rod-shaped cells by applying pressure on the coverslip (Figure 2, A and B). This caused the cross section of the cell and the septum hole to take on a flat-oval shape. The cross section of the cell, as marked by fluorescein isothiocyanate conjugated lectin (FITC-lectin), did not change over the course of the experiment (Figure 2B). Time-lapse imaging showed that the septum continued to grow (Figure 2B). Of interest, the septum hole grew from its original flat-oval shape into a more-rounded shape, indicating that the growth of the septum was not homogeneous (Figure 2B). The septum grew 4.0 ± 1.8 times faster in the direction of the long axis than along the short axis. The curved part of the septum grew faster than the flat part

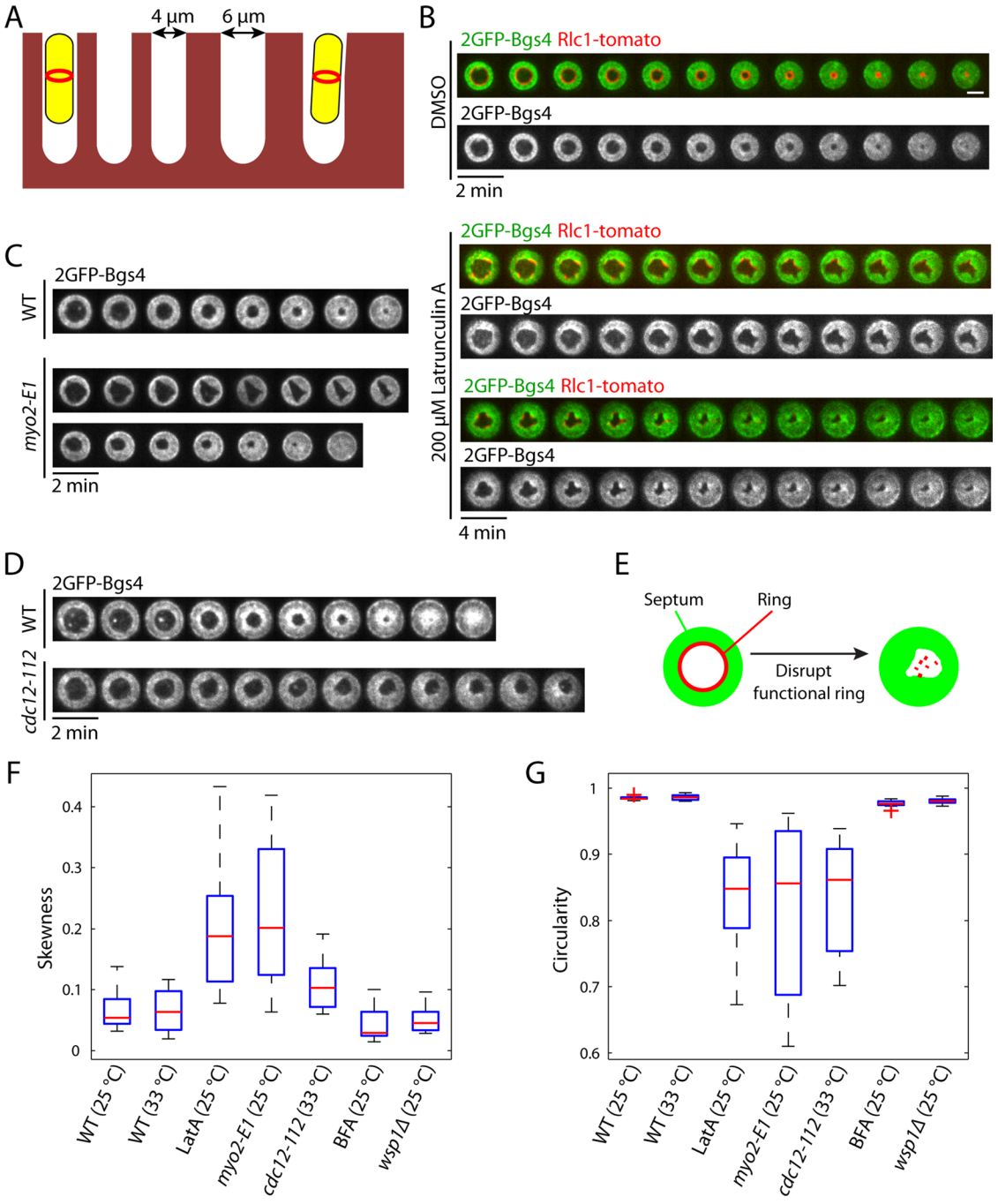

FIGURE 1: Spatial coordination of septation by the cytokinetic ring. (A) Schematic of fission yeast cells standing vertically in micro-well PDMS chambers. (B) Time-lapse images of wild-type live cells. 2GFP-Bgs4 and Rlc1-tomato expressed from their native promoters were used to mark the septum and the cytokinetic ring, respectively. Cells were grown at 25°C and imaged with 2-min intervals. Sum of intensity projection of confocal images of the medial three slices. Top, cells treated with DMSO imaged as a control at 2-min intervals. Note that the septum hole was round and symmetric throughout the whole process. Bottom, cells treated with 200 μM LatA imaged at 4-min intervals. Note that the septum hole becomes noncircular and asymmetric. (C) Time-lapse images of *myo2-E1* (myosin heavy chain) mutant cells expressing 2GFP-Bgs4, grown at 25°C. (D) Time-lapse images of *cdc12-112* (formin) mutant cells expressing 2GFP-Bgs4. Cells were initially grown at 25°C and then shifted to 33°C for imaging. Scale bar, 2 μm. (E) Schematic showing septation in the absence of a functional ring. (F, G) Boxplots of skewness and circularity of septum holes from cells of various strains and treatments ($n \geq 7$ cells; see *Materials and Methods*). (F) Quantification of the skewness of septum holes for each condition (see *Materials and Methods*). (G) Quantification of the circularity of septum holes for each condition (see *Materials and Methods*). See also Supplemental Figure S1.

(Figure 2, C and D). By varying the extent to which we flattened the cells, we observed that the initial height of the septum hole negatively correlated with the ratio between the septum growth rates along the long and short axes (Supplemental Figure S2). Thus these findings suggest that the shape of the septum hole may modulate the local growth of the septum.

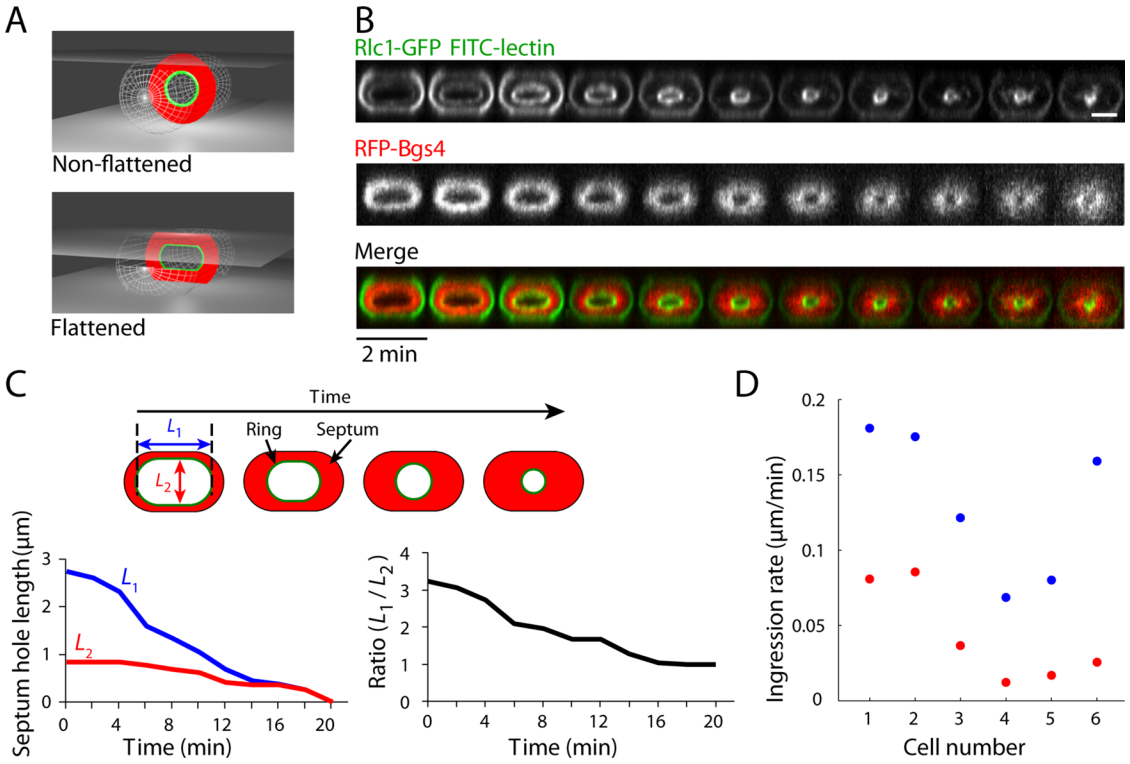

FIGURE 2: Septum closure in flattened cells. (A) Fission yeast cells were placed between a glass coverslip and glass slide in liquid medium and gently pressed to produce a flattened shape. Schematic view, with the septum in red and ring in green. (B) Time-lapse images of a representative wild-type live flattened cell expressing RFP-Bgs4 and Rlc1-GFP. 3D projections of the confocal images. Cells were stained with FITC-lectin to mark their boundaries. Images were taken at 2-min intervals. Note the change of the shape of the septum hole. Scale bar, 2 μm. (C) Quantification of septum ingression in a representative cell. Note that the septum ingresses faster along the long axis than along the short axis. (D) Comparison of ingression rates along the long and short axes in different cells. Blue dots, long axis; red dots, short axis. Note that the septum ingresses faster along the long axis than the short axis in each case. See also Supplemental Figure S2.

Second, we placed cells vertically into PDMS chambers and then stretched the PDMS slab. In this procedure, the cross section of the cells and the division apparatus became oval shaped (Figure 3A and Supplemental Figure S3). Time-lapse images showed that the oval septum also ingressed faster along the long axis than along the short axis (Figure 3B). Oval shapes were maintained with a roughly consistent speed ratio between the axes (Figure 3, C and D). To address the possibility that effects were due to compression of the septum caused by the manipulations, we found similar behavior in cells that formed a septum only after the cells were deformed (Supplemental Figure S3B). Imaging of these oval-shaped cells in a vertical orientation allowed us to measure the distribution of division proteins. The mean fluorescence intensities of Rlc1-tomato on the ring and GFP-Bgs4 along the septum leading edge were uniform (Figure 3E). In particular, in individual cells, fluorescence intensities at regions at the long axis and at the short axis showed no differences (average ratio of Bgs4 intensities, 1.00 ± 0.07; ratio of Rlc1 intensities, 0.95 ± 0.12; $n = 6$). Therefore the asymmetric rates of septum growth along these oval-shaped septa were not due to differences in the distribution of these proteins.

Third, we generated irregular shapes of the septum hole using the formin *cdc12-112* temperature-sensitive mutant. On shift to restrictive temperature, *cdc12-112* cells rapidly lose their actomyosin ring (Pelham and Chang, 2002), and the septum holes become irregular in shape. When shifted back to the permissive temperature, the cells reformed an actin ring in ~5 min (Figure 4A). We used this procedure to determine whether an irregularly shaped septum can become more circular over time (Figure 4B). Indeed, we observed that the septum hole gradually grew into a more circular shape in the presence of an actin ring (Figure 4C; in four of five cells observed). This is caused by differences in the local growth rates of the septum cell wall along the septum leading edge (Figure 4D). Taken together, our data suggest that variations in local ingression rate may be generally a function of the septum hole shape regardless of the initial shape and act to drive the septum hole toward a circular cross section.

Septal growth rate is dependent on local curvature

These experiments suggest that in the presence of a functional ring, local septum growth rates depend on the local shape of the septum, with increased cell wall growth at curved regions of the septum hole. This result can be explained if the rate of cell wall assembly is mechanosensitive to the pulling force of the ring normal to the membrane. Generalized from the law of Laplace (Laplace, 1805; Evans and Yeung, 1989; Dai and Sheetz, 1999; Zhang and Robinson, 2005), the amount of force perpendicular to the membrane is dependent on the tension along the membrane (generated by the contractile force of the ring attached to the membrane) and is proportional to the local curvature (Thiyagarajan *et al.*, 2014). The roughly equal distributions of myosin and actin filaments around the ring (Figure 3E; Motegi *et al.*, 2000; Kamasaki *et al.*, 2007) suggest that tension in the plane of the membrane is roughly equal along the septum. Thus, in

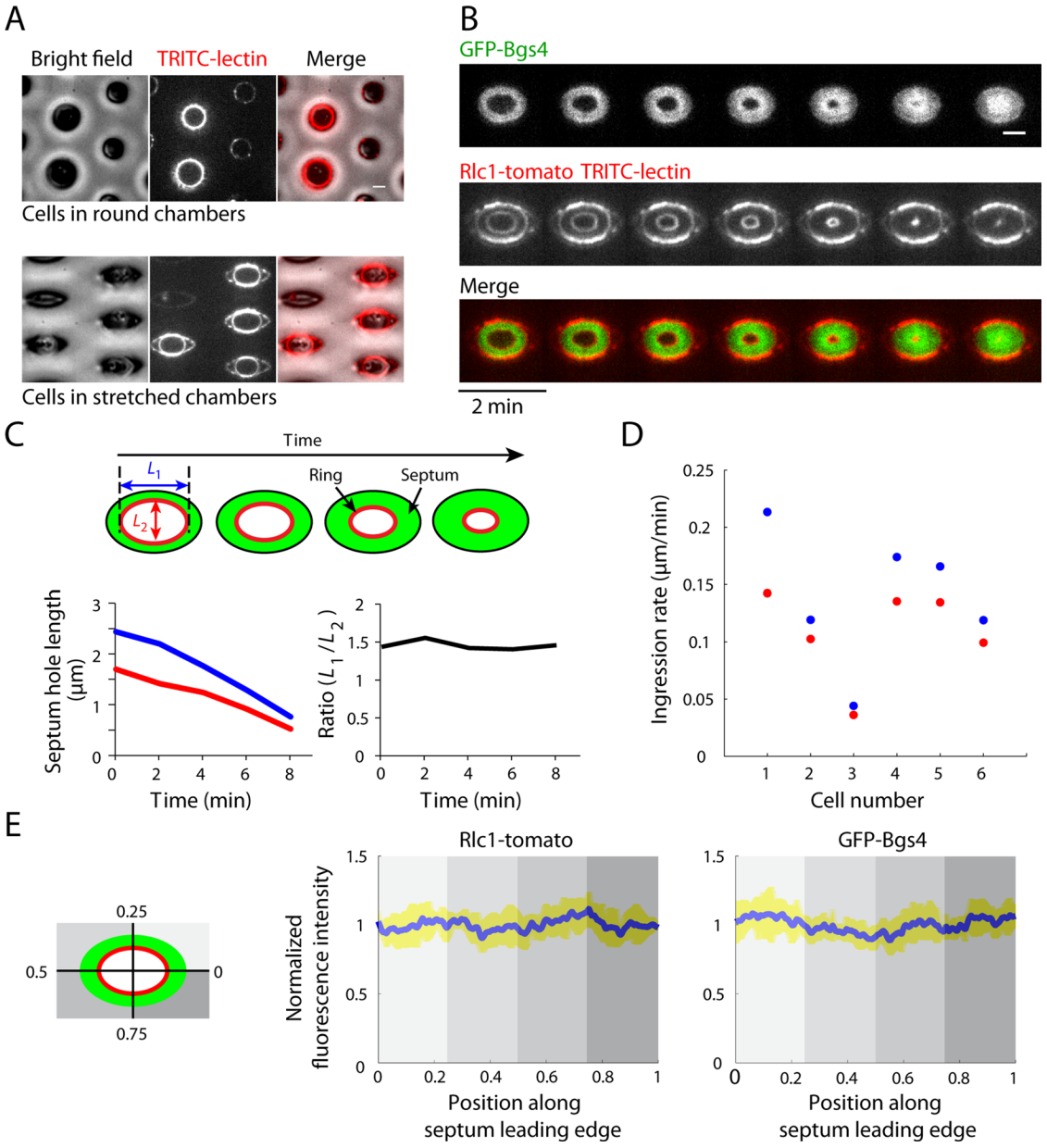

FIGURE 3: Septum closure in cells with an elliptical shape. (A) Fission yeast cells were placed vertically in PDMS wells as in Figure 1A. The PDMS slab was then physically stretched in one direction (Supplemental Figure S3A), deforming the wells and the cells, which take on an oval-shaped cross section. TRITC-lectin stains the cell walls and fortuitously the edges of the PDMS chambers, and GFP-Bgs4 and Rlc1-tomato mark the septum and the cytokinetic ring, respectively. (B) Time-lapse images of wild-type live deformed cells. Sum of intensity projection of the confocal images. Scale bar, 2 μm. (C) Asymmetric septum closure in a representative cell. (D) Comparison of ingression rates along the long and short axes in different cells. Blue dots, long axis; red dots, short axis. (E) Measurements of fluorescence intensities of Rlc1-tomato and GFP-Bgs4 around the leading edge of the septum. Left plot, Rlc1-tomato; right plot, GFP-Bgs4. Fluorescence intensity values were normalized to the mean intensity along each septum. Graphs show average values with SD as error bars ($n = 6$ cells). See also Supplemental Figure S3.

this case, force should simply correlate with curvature. This relationship predicts that in regions with high curvature, the cytokinetic ring exerts higher inward pulling force on the plasma membrane, whereas in the flat regions, the ring provides little inward pulling force.

To test this mechanical model, we sought to quantify the relationship between local septum growth and curvature. We measured the local curvature and the local septum growth rate via a semiautomatic MATLAB script based on contour-tracking software (Ursell *et al.*, 2014). Consecutive contours of the septum hole were extracted at subpixel resolution from time-lapse images (see *Materials and Methods*). As a control, we examined an ideal case in which we computationally generated contours of septum holes that are concentric circles with similar spatial resolution to our experimental measurements. As expected, local curvatures and local growth rates were essentially constant, leading to a cluster of data points around one focus (Figure 5A). Experimental data from wild-type cells showed a similar distribution (Figure 5B), reflecting the centripetal closure of a circular septum.

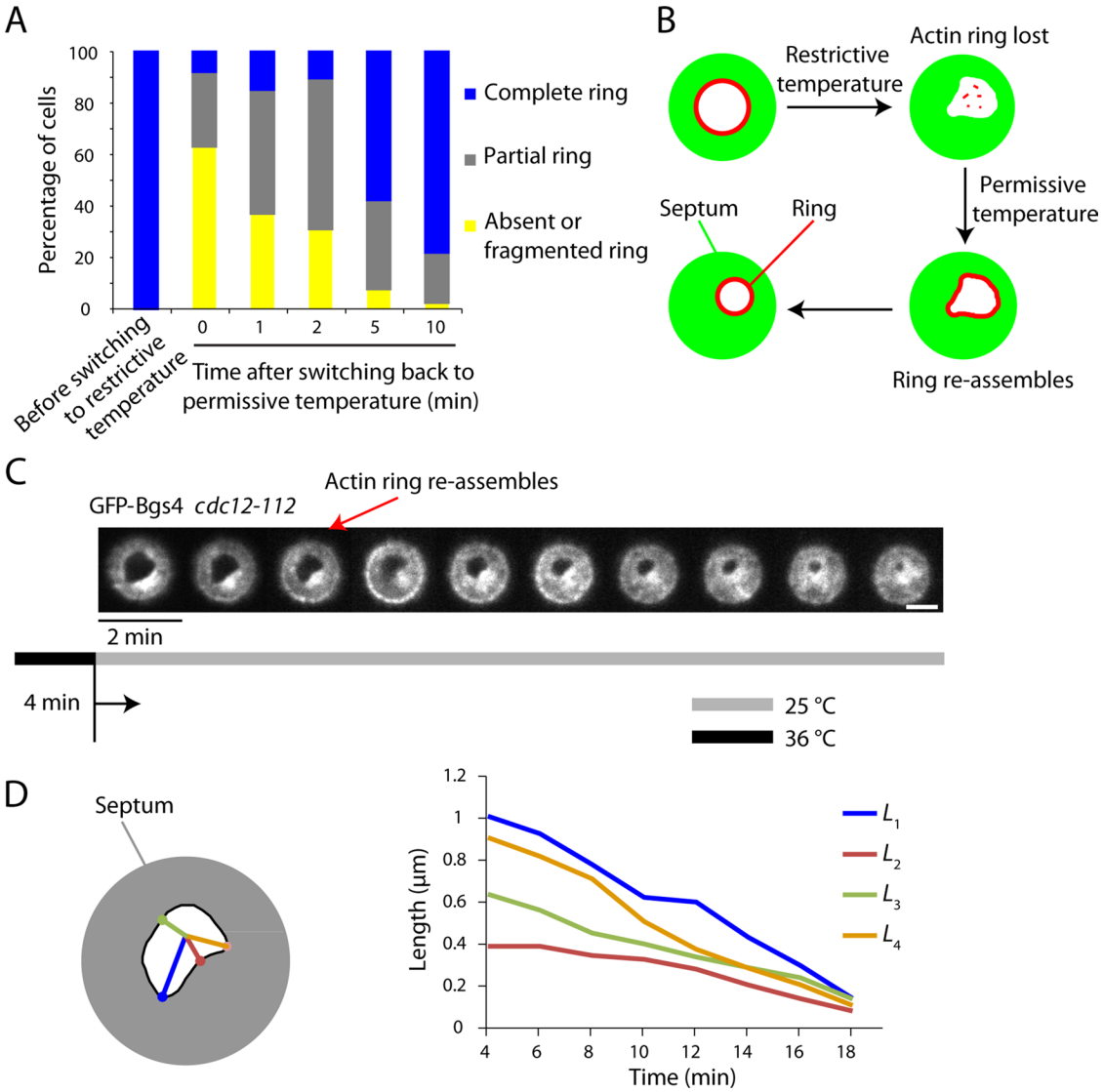

FIGURE 4: Asymmetric growth of irregularly shaped septa in *cdc12-112* formin cells. (A) Irregularly shaped septa were generated in formin *cdc12-112* temperature-sensitive mutant cells by growing them at the permissive temperature of 25°C, shifting to the restrictive temperature 36°C for 4 min to inhibit the ring, and then going back to 25°C for various lengths of time. Samples were prepared, fixed, and stained for F-actin and DNA (Supplemental Figure S4). Graph shows percentage of cytokinesis-phase cells with a complete, partial, or absent/fragmented actin ring. Note that the actin rings appear to reassemble in most cells after ~5 min at the permissive temperature. (B) Schematic showing the operation of *cdc12-112* cells and changes in the actin ring and the septum shape. (C) Time-lapse images of a representative *GFP-Bgs4 cdc12-112* cell after being transferred to the restrictive temperature and then restored to the permissive temperature. Note that starting from 6 min, the septum hole gradually grows more regular in shape. Scale bar, 2 μm. (D) Quantification of septum growth of the *cdc12-112* cell in C. The distance labels L_1, L_2, L_3, and L_4 are color coded as indicated in the diagram on the left. Note that the local ingression rate is greater at the regions with higher curvature.

However, analyses of time-lapse images of cells with altered septum shapes revealed a range of local growth rates. Strikingly, local growth rates across the septum hole boundary in a given cell showed a strong positive correlation with the measured local curvature in flat-oval and oval-shaped septa (Figure 5, C and D). A positive but somewhat weaker correlation was evident in the irregularly shaped septa (*cdc12-112* cell; Figure 5E); the weaker correlation coefficient values may reflect the incomplete recovery of a functional ring in this condition. In contrast, in LatA-treated cells without an actin ring, the correlation was lost (Figure 5F). These observations suggest that septum growth is dependent on local curvature and that this property is dependent on the cytokinetic ring (Figure 5G).

Mathematical modeling of septum growth based on curvature dependence

To test whether curvature-dependent growth is sufficient to recapitulate the trajectories of septum hole shape that we observed in our various perturbations, we developed a mathematical model to simulate the process of septum ingression. We assume that the local growth rate of the septum scales proportionally with local curvature. In simulations based on this model, qualitative comparisons of

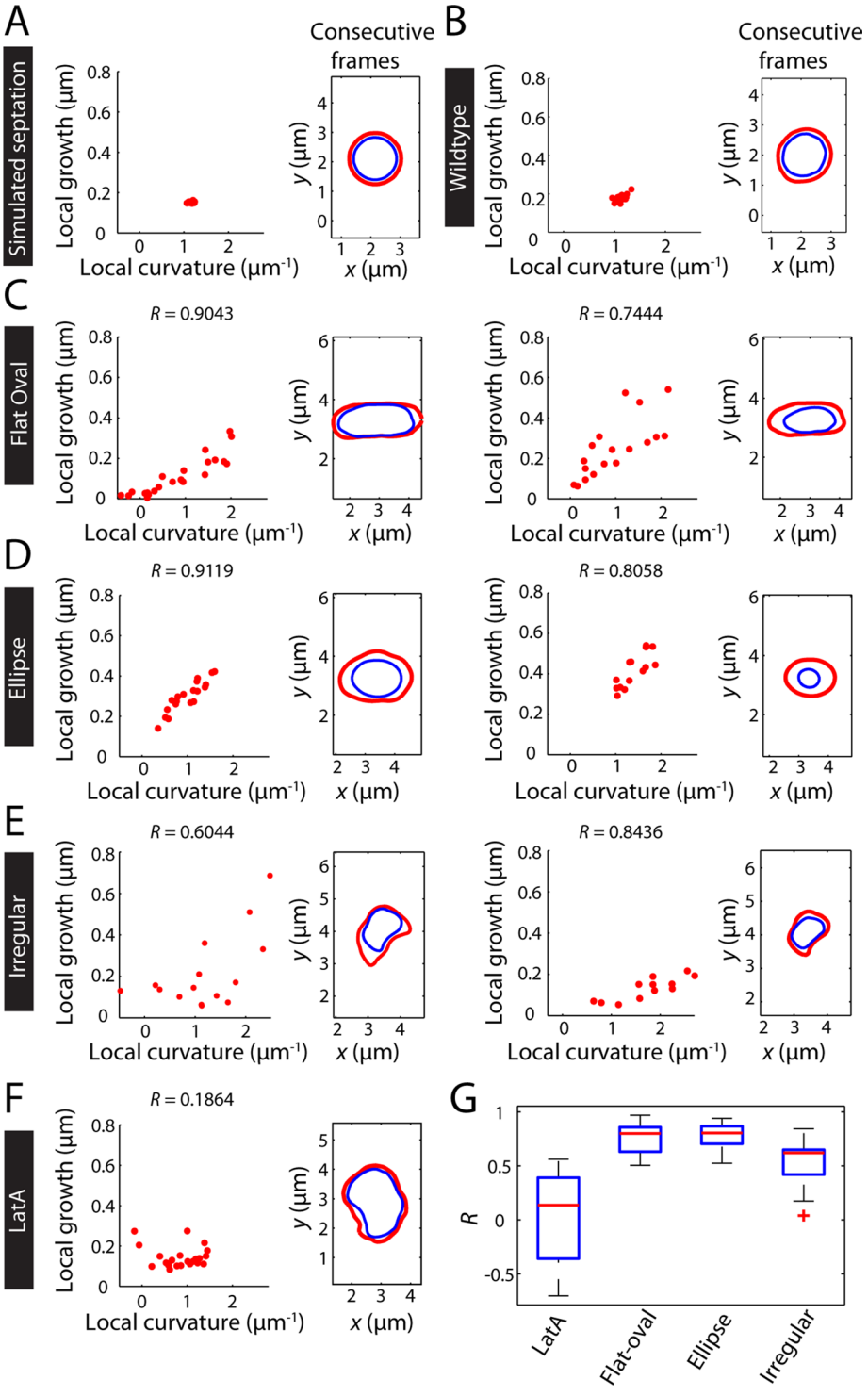

FIGURE 5: Growth of the septum cell wall correlates with local curvature. Contours of closing septum holes were extracted and analyzed for local cell wall growth and local curvature. The left scatter plots compare the local curvature during septum ingression vs. local growth (see *Materials and Methods*). The right plots show the contours of each septum at the two consecutive time points used for the scatter plot (4 min apart in A–E and 12 min apart in F). (A) Simulated septation (ideal circular images were created and processed using the foregoing methods); (B) wild-type cells during normal growth; (C) cells with flat-oval septum holes as in Figure 2; (D) cells with elliptical septum hole as in Figure 3; (E) *cdc12-112* cells with irregularly shaped septum holes as in Figure 4; and (F) wild-type cells treated with 200 μM LatA. (G) Comparison of correlations. Average Pearson correlation coefficients (R) from plots like those given were generated from $n \geq 12$ time points in two or three image sequences for each treatment group.

septum hole shape showed that the model largely recapitulated experimental results (Figure 6, A with D; B with E; C with F); quantitative comparison between the shapes in our simulations and those extracted from experimental data exhibited a high area of overlap and low comparison error (Supplemental Figure S5A and Figure 6, J–L, black line). This agreement for simulations of curvature-dependent growth was present across cells with different septum hole shapes and during the progress of ingression for single cells. In contrast, in simulations in which the septum ingressed uniformly along the septum leading edge, the septum hole did not become circular during progression (Figure 6, G–I) and the errors of simulation are higher (Figure 6, J–L, red line). Thus, our simulations demonstrate that curvature-dependent regulation of septum growth can explain the patterns of septum growth seen in the different experiments.

Local concentrations of ring components may also contribute to septum assembly

We next examined why the septum grows into irregular shapes in the absence of the functional ring. In the absence of actin, many ring components remain associated with the division site, presumably by association with the plasma membrane (Naqvi *et al.*, 1999; Wu *et al.*, 2003). In LatA-treated wild-type cells labeled with Rlc1-tomato and 2GFP-Bgs4, Rlc1-tomato in the ring appeared to fragment into numerous pieces on the membrane. We found that the septum locally grew faster at regions containing these Rlc1-tomato fragments (Figure 7A; see also Figure 1B). These regions are likely to contain many ring proteins, including Cdc12 (Figure 7C) and Cdc15 (Supplemental Figure S6A). This correlation suggests that fragments containing a subset of ring proteins may promote local septum growth. One candidate that might drive septum growth is Bgs1, a β-glucan synthase that drives primary septum formation (Cortes *et al.*, 2007). Of interest, in LatA-treated cells and in *myo2-E1* mutants, the distribution of GFP-Bgs1 is heterogeneous (Figure 7D and Supplemental Figure S6D), and the rate of local septum growth correlates with the local intensity of GFP-Bgs1 (Figure 7D and Supplemental Figure S6D). Therefore, in contrast to septum formation in oval-shaped cells, in which the ring exhibited even distributions of components (Figure 3E), in these LatA-treated cells or *myo2-E1* mutants, the asymmetric distributions of ring components such as Bgs1 influence the spatial control of septum assembly.

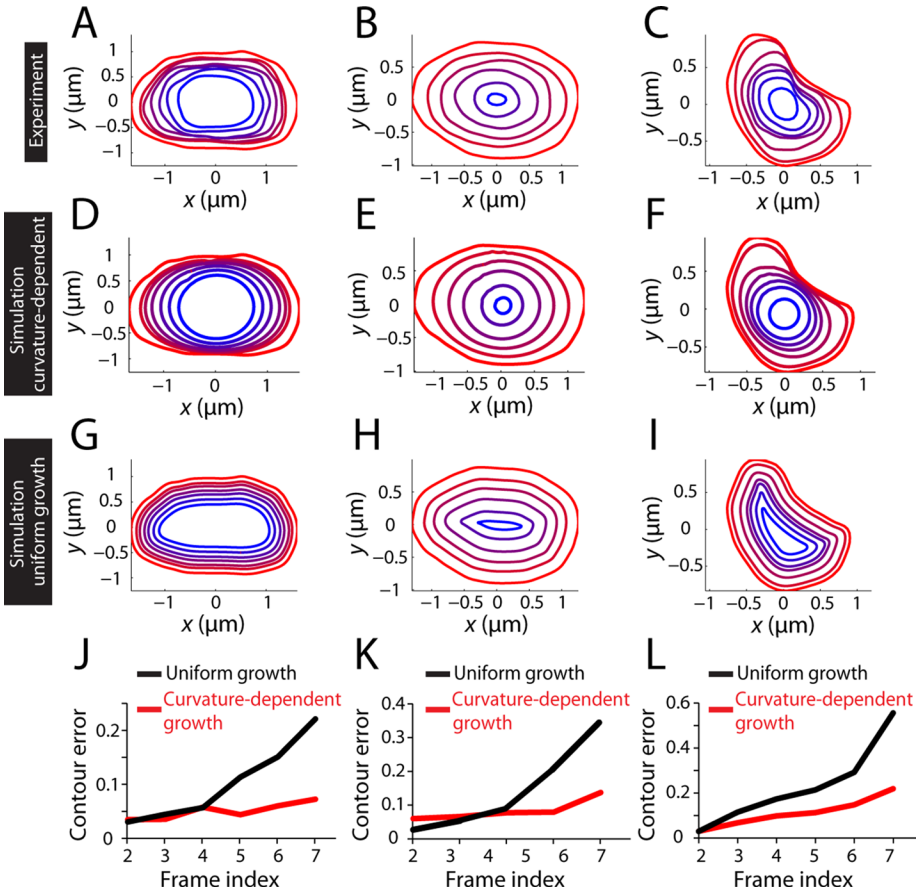

FIGURE 6: Mathematical simulations of septum morphologies based on curvature-dependent growth. (A–C) Experimental data showing contours of septum holes in time-lapse sequences in (A) cells with flat-oval septum holes as in Figure 2, (B) cells with elliptical septum holes as in Figure 3, and (C) cells with irregularly shaped septum holes as in Figure 4. Contours were extracted from the time-lapse images of septum ingression and were projected onto the same two-dimensional (2D) plane. The interior contours (more blue) are later time points of septum ingression than the exterior contours (more red). (D–F) Simulations of septum growth assuming curvature-dependent growth. The initial contours were taken from the initial frames for the corresponding cell in A–C. The local septum growth direction was determined by the average normal over 326.5 nm (5 pixels); the local septum growth rate was determined based on the local curvature and their positive correlation (see *Materials and Methods*). All generated contours were projected onto the same 2D plane. (G–I) Simulations of septum growth assuming uniform growth. The local septum growth direction was determined by the average normal over 400 nm; the local septum growth rate was uniform (see *Materials and Methods*). (J–L) Comparison between experimental results and simulations. The error of each frame was calculated from the contour of the experimental result and the corresponding simulated contour with curvature-dependent (red) and uniform (black) growth (see *Materials and Methods*). See also Supplemental Figure S5.

DISCUSSION

The contractile ring regulates curvature-dependent septum assembly

Here we showed that the *S. pombe* contractile ring spatially coordinates the process of septum formation, leading to a circular, centered septum hole (Figures 2–4). In the absence of F-actin or other ring components, the septum assembles in a disorganized manner and adopts highly noncircular shapes (Figure 1). In cells with a noncircular septum, the division machinery in the presence of a functional ring appears to employ a correction mechanism that makes the shape of the hole more circular as the septum ingresses, in an actin-dependent manner. Our experimental measurements coupled with modeling demonstrate that the dynamics of this shape restoration are consistent with curvature-dependent septum growth. We speculate that the ability of the ring to globally coordinate cell wall synthesis is critical for the orderly and accurate formation and closure of the cell wall for proper division. Even in cells of normal morphology, the ring may be needed to correct for natural variations in cell wall synthesis around the septum (Thiyagarajan *et al.*, 2014). As illustrated by ring and cell wall mutants (Chang *et al.*, 1996; Mishra *et al.*, 2004; Cortes *et al.*, 2005; Wu *et al.*, 2010), orderly assembly of the septum is critical for cell integrity during division: if septum assembly is disorganized and the cell wall is not complete, there is a danger of the cell stalling in cytokinesis or lysing if it attempts to divide.

The strong positive correlation between septum growth rate and hole curvature in a variety of morphological situations (Figure 5) suggests that the cytokinetic ring regulates septum assembly using a force-sensitive mechanism. The ability of contractile structures to shape membranes is well known. However, in this case, it is likely that the ring is not the primary force generator for ingression; calculations suggest that the ring cannot exert nearly enough force to counter turgor pressure for division (Proctor *et al.*, 2012). Instead, the ring likely provides a relatively small amount of pulling force on the plasma membrane. The forces perpendicular to the membrane are predicted to be curvature dependent: in regions with higher curvature, the cytokinetic ring should exert higher inward pulling force on the plasma membrane than in flat regions parallel to the plasma membrane. How mechanical force stimulates cell wall synthesis is not yet clear. One possibility is that actin filaments in the ring may pull directly on a glucan synthase such as Bgs1 or one of its regulators or pull on the membrane (Proctor *et al.*, 2012). It is unlikely that the local curvature of the membrane itself explains these shape effects, as a much larger curvature along the long axis of the cell at the edge of the septum is likely to dominate the more subtle changes in curvature along the septal hole. The basis for mechanical regulation of cell wall synthases will be an interesting question to pursue.

This simple curvature-based model does not account for all properties of ring closure. Of note, cleavage furrow ingression in many cell types has been noted to occur at a constant rate (Pelham and Chang, 2002; Carvalho *et al.*, 2009); a model based purely on curvature predicts that closure would gradually speed up as curvature increases during ingression. Further, the rate of ingression scales with the initial size of the ring (Carvalho *et al.*, 2009; Calvert *et al.*, 2011). To explain these behaviors, a model based on contractile units, in which the architecture of the ring changes as it closes, has been proposed (Carvalho *et al.*, 2009); in the context of

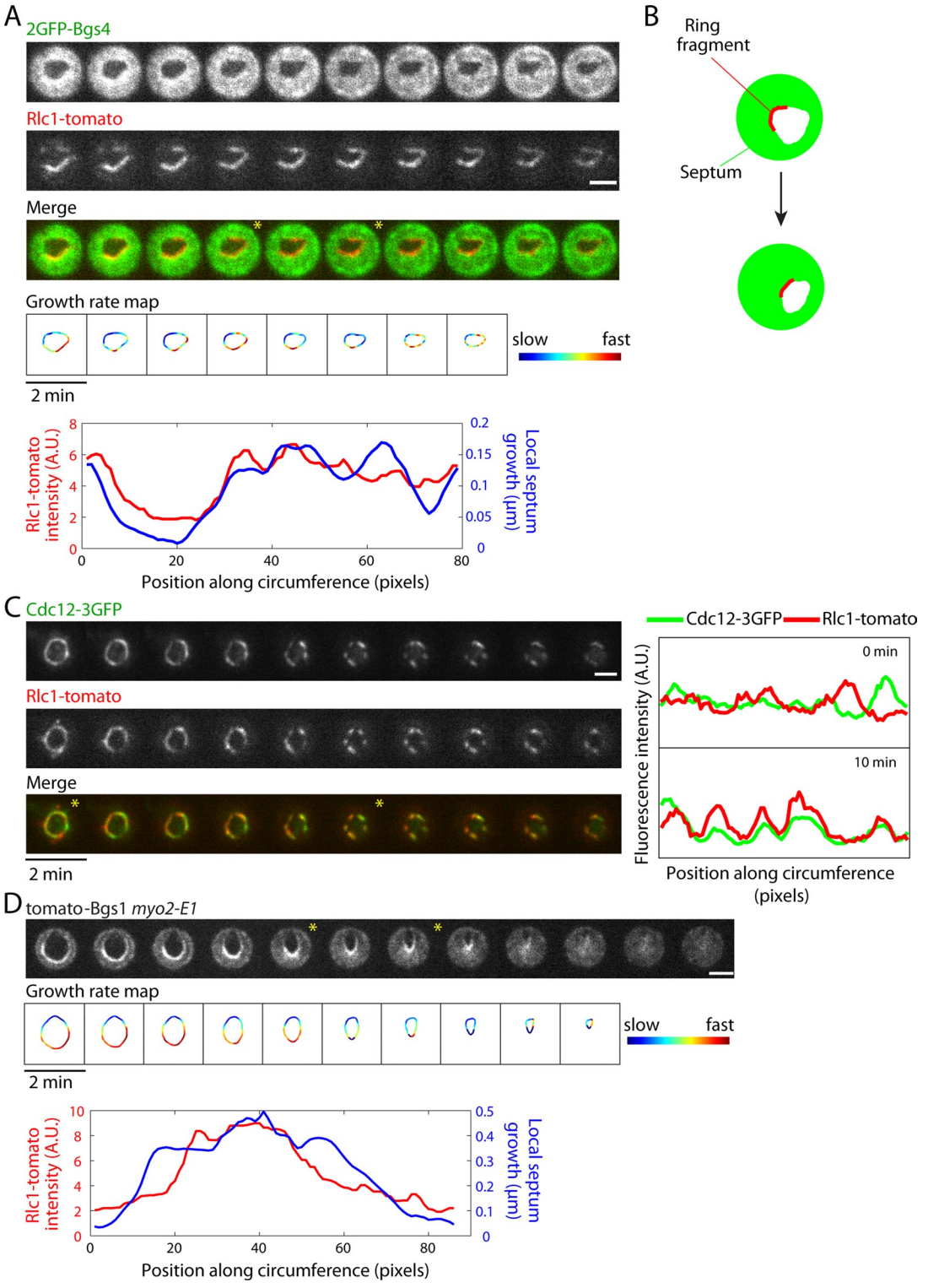

FIGURE 7: Ring fragments locally stimulate septum growth in the absence of the ring. (A) Time-lapse images of live wild-type cells expressing Rlc1-tomato and 2GFP-Bgs4 treated with 200 μM LatA. Growth rate maps of septum assembly were generated from the contour of the septum hole of the image at the current time point and the contour 4 min later. Local growth amount was measured using the same method as in Figure 3. Heat map represents the relative local growth rate. Bottom, local growth of the septum (frames 4–6) and the corresponding distribution of Rlc1-tomato fluorescence intensity (frame 4). (B) Schematic showing that local septum growth correlates with localization of cytokinetic ring components in the absence of a functional ring. (C) Time-lapse images of wild-type cells expressing Cdc12-3GFP (formin) and Rlc1-tomato (regulatory myosin light chain) treated with 200 μM LatA. Note that these proteins still colocalize upon fragmentation of the ring. (D) Time-lapse images of *myo2-E1* cells expressing Tomato-Bgs1 (β-glucan synthase). Growth rate maps and comparison between septum growth and Tomato-Bgs1 distribution in frames 5–7 are as described in A. Scale bar, 2 μm. See also Supplemental Figure S6.

this model, changes in contractile forces may offset the effects of the increase in curvature as ingression proceeds.

It is now apparent that the cytokinetic ring has multiple roles in cytokinesis. Previous studies showed that the ring is needed for initial marking of the septum site and determines the position and orientation of the division plane. However, how the ring recruits the cell wall machinery to this site is not well understood. Here we examined its roles during closure, after septation has started. We find that in addition to force production, the ring has additional functions in stimulating cell wall synthesis. In LatA-treated cells, a subset of ring components still localize to the division site in fragments (Figure 7; Wu *et al.*, 2003). Similar abnormal structures have been noted in animal cells (Hickson and O'Farrell, 2008). In fission yeast, these fragments are able to promote septum growth, but in an uneven manner. Thus, in addition to mechanical forces, the ring also serves to spatially distribute the cell wall machinery relatively evenly around the leading edge of the plasma membrane.

Actin and cell shape regulation

These findings provide an example of how contractile structures may use force to globally influence cell shape, in this case to shape the septum into a round annulus. During cytokinesis in animal cells such as sea urchin, the contractile ring is believed to provide the major force for pulling in the plasma membrane for furrow ingression (Rappaport, 1967). However, there has been little quantitation of ring shapes during ingression that could be used to directly test such mechanical models. Using an approach similar to the one we presented here, we found that sea urchin embryonic cells also generate patterns of closure that are based on curvature dependence (unpublished data)—for instance, closing a triangular hole into a round one. In these cells, the contractile ring may provide curvature-dependent forces to directly move the membrane. Similar membrane closure events guided by purse-string actin structures have also been studied in systems such as epithelial wound closure in *Drosophila* embryos (Abreu-Blanco *et al.*, 2012) and wound closure in *Xenopus* eggs (Mandato and Bement, 2001).

In walled cells, there is a growing appreciation for the links between cell wall assembly and guidance by the underlying cytoskeleton. In bacteria, FtsZ (tubulin-like) and FtsA actin-like (Bork *et al.*, 1992) recruit downstream proteins to guide cell wall assembly and remodeling during cell division (Lutkenhaus *et al.*, 2012; Typas *et al.*, 2012). The actin-like MreB localizes to sites of cell wall assembly along the lateral cell walls of rod-shaped bacteria during cell elongation, and its dynamics is dependent on cell wall synthesis (van Teeffelen *et al.*, 2011; Typas *et al.*, 2012; White and Gober, 2012). In plants, cellulose synthase complexes are similarly guided by cortical microtubules (Paredez *et al.*, 2006; Gutierrez *et al.*, 2009). Mechanical stresses regulate cell wall shapes and may regulate microtubule distribution (Landrein and Hamant, 2013). In cytokinesis of higher plants, microtubules at the phragmoplast position the formation of the cell wall plate at cytokinesis, and actin appears to guide cell wall growth to position and orient the plate (Schmit and Lambert, 1988; Valster *et al.*, 1997; Smith, 1999). Understanding how mechanics and the cytoskeleton control the cell wall will be a key to understanding cell shape control in walled cells.

MATERIALS AND METHODS

Yeast strains and media

Standard methods for media and genetic manipulations were used. *Schizosaccharomyces pombe* strains used in this study are listed in Supplemental Table S1. Cells were generally grown at 25°C in rich YE5S (yeast extract with amino acid supplements; Sunrise Science Products, San Diego, CA) medium to exponential phase.

Microfabrication of wells

Soft lithography methods were used to make PDMS microwells of varying diameters and spacings. These were cylindrical wells of 4-6 µm in diameter, with ~20-µm depth in a hexagonal array. The photo mask design was generated as printed chrome on mica by Advance Reproductions Corporation (North Andover, MA), and a silicon master was fabricated using standard photolithography techniques at the Microsystems Technology Laboratory at the Massachusetts Institute of Technology. A 10:1 mixture of PDMS SYLGARD 184 silicone elastomer and curing agent (Dow Corning, Midland, MI) was poured onto a master and subsequently baked at 50°C for 6 h. The replica was then peeled off the master. The PDMS wells were treated with a plasma cleaner (Harrick Plasma, Ithaca, NY) for 1–2 min just before addition of the cells.

Microscopy

A spinning-disk confocal (CSU10; Yokogawa, Tokyo, Japan) inverted microscope (Eclipse Ti; Nikon, Melville, NY) with a Hamamatsu electron-multiplying charge-coupled device camera (Hamamatsu Photonics, Hamamatsu, Japan) and 100×/1.4 numerical aperture objective with a 1.5× magnifier was used for image acquisitions. Imaging was performed at room temperature (25°C) unless otherwise indicated. When necessary (imaging *cdc12-112* strains), temperature was controlled using an objective heater (Bioptechs, Butler, PA). Image acquisition was performed using Micromanager 1.4 (Edelstein *et al.*, 2010).

For imaging cells with a conventional orientation such that the septum is perpendicular to the imaging plane, confocal slices were taken at 0.4-µm intervals. The raw images were then either processed through 3D projection or flattened using maximum-intensity projection.

For inserting cells into PDMS chambers, cells growing in exponential phase were concentrated 25 times by spinning for 10 s, and 1 µl of concentrated culture was spread onto the PDMS chambers. The sample was then covered with a coverslip on which gentle force was exerted to push the cells in. Typically 10–50% of the wells could be filled with individual cells. The fields were manually scanned for cells with a ring, and then cells were followed by time-lapse imaging. The focus was set at the medial focal plane around the septum. Three *z*-slices 0.4 µm apart centered at the medial focal plane were acquired to cover the entire septum. Images used for analysis were sum-intensity projections of these three slices.

Dyes

Alexa Fluor 488–Phalloidin (Molecular Probes, Life Technology, Eugene, OR) was used for F-actin staining in fixed cells (Chang *et al.*, 1996). 4′,6-Diamidino-2-phenylindole (DAPI) was added at a concentration of 1 µg/ml for nucleus staining. Cell wall was stained with FITC-lectin (Sigma-Aldrich, St. Louis, MO; Figure 2) or tetramethylrhodamine isothiocyanate–conjugated lectin (TRITC-lectin; Sigma-Aldrich; Figure 3).

Pharmacological inhibitors and drugs

LatA (Sigma-Aldrich) assays were performed by concentrating 500 µl of cell liquid culture into 49.5 µl and adding 20 mM LatA stock in dimethyl sulfoxide (DMSO) for a final concentration of 200 µM. At this concentration, we confirmed that there was no F-actin detectable by phalloidin staining in the cell. BFA (Sigma-Aldrich; Turi *et al.*, 1994) was prepared in ethanol (10 mg/ml) and kept at

4°C, and this stock was used as a 100-fold dilution to the final concentration of 100 µg/ml.

Image analysis

Image processing was done using ImageJ (National Institute of Health, Bethesda, MD) and MATLAB R2009b (MathWorks, Natick, MA). Images in a time-lapse sequence were preprocessed using the ImageJ plug-in StackReg (Thevenaz *et al*., 1998).

To quantify skewness and circularity, contours of the septum holes and the outline of the cells were extracted manually using ImageJ. Skewness is defined as the ratio between the distance of two mass centers and the radius of the circle fit to the cell, where positions of the mass centers were calculated using ImageJ. Circularity is defined as follows:

$$\text{circularity} = \frac{4\pi \times \text{area}}{\text{perimeter}^2} \quad (1)$$

where area and perimeter are those of the septum hole and were calculated using ImageJ. The data in Figure 1 are box plots, in which the red bar marks the median; the box contains the 25th (q1) to 75th (q3) percentiles, and the whiskers extend to the most extreme data that are not outliers, which are defined as smaller than 2.5q1 – 1.5q3 or greater than 2.5q3 + 1.5q1.

To measure local septum growth and curvature, contours were extracted either using a custom MATLAB script (Ursell *et al*., 2014; Figure 5, A, B, and D) or by hand using a customized script written in MATLAB to allow subpixel resolution (Figure 5, C, E, and F) and then followed by Gaussian smoothing (SD, 10 pixels; Gaussian mask, 3 pixels). Midplane contour curvature was a three-point measurement defined by the arc-length derivative of the vector field formed from the unit normals to the contour. Each curvature profile was smoothed with a low-pass Gaussian filter with SD $\sigma = 10$ contour points and Gaussian mask $r = 60$ points. There is effectively no lower bound on the magnitude of curvature that can be measured, whereas we estimate that optical limitations and the smoothing filter impose a limit on the maximum magnitude of measured curvature of no more than ~7 μm^{-1}. Across a wide range of cellular data, the observed curvatures range from ~0 to ~3 μm^{-1} and thus lie within the resolution limits. Local growth direction was determined by calculating the mean surface normal over 326.5 nm (5 pixels). Local growth rate was calculated from the distance between two consecutive frames (4 min apart) at a point in the direction of local growth (normal to the contour at the earlier time point).

Local protein fluorescence intensity at the leading edge of the septum was measured by adding up the intensity value of the pixel over the septum contour and the intensity values of its 4 adjacent pixels along the normal direction (2 pixels outside and 2 pixels inside).

The area within a closed contour was calculated using the built-in MATLAB "polyarea" function.

Mathematical simulations of septum ingression

Mathematical simulations of septum ingression were carried out in MATLAB. Septum curvature and septum growth direction were determined using the same method as for experimentally determined contours. Local septum growth rate was assumed to either be curvature-dependent (Eq. 2) or uniform along the leading edge of the septum. For curvature-dependent simulations, the local ingression rate v was given by

$$v = c\kappa \quad (2)$$

where c is a constant and κ is the local curvature of the septum. If the local curvature was negative, growth was set to 0.

To increase simulation accuracy, the points extracted from the contour were locally linearly interpolated with a distance of 0.1 pixel.

Raw growth direction vectors $\vec{d'}$ were obtained by calculating the normal vector of the tangent of three adjacent points across the extracted contour. The raw growth direction always points to the inside of the septum hole. Growth direction vectors $\vec{d}$ were then calculated by averaging $\vec{d'}$ over 51 points. For each contour point, the position ($\vec{p_i}$) was updated at each iteration of the simulation as

$$\vec{p_i}(t + dt) = \vec{p_i}(t) + v\vec{d_i} \quad (3)$$

After each iteration, we respaced the points along the contour using interpolation to maintain a uniform distance between points. An example of the simulation showing each iteration can be seen in Supplemental Figure S5B. Figure 6 shows the representative frames.

Error from the comparison of the simulated contour and the experimental data are calculated using

$$1 - \frac{2A_{\text{overlap}}}{A_{\text{experiment}} + A_{\text{simulation}}} \quad (4)$$

The overlap of two closed contours was calculated using the MATLAB "polybool" function.

ACKNOWLEDGMENTS

We thank the Chang lab for support and useful discussions, S. Thiyagarajan and B. O'Shaughnessy for discussion and communication of results before publication, J. C. Ribas and M. Ramos for strains, and the Marine Biology Laboratories Whitman Investigator Program for facilitating collaborations. This work was supported by National Institutes of Health New Innovator Award DP2OD006466 to K.C.H. and Grant R01 GM056836 to F.C.

REFERENCES

Abreu-Blanco MT, Verboon JM, Liu R, Watts JJ, Parkhurst SM (2012). Drosophila embryos close epithelial wounds using a combination of cellular protrusions and an actomyosin purse string. J Cell Sci 125, 5984–5997.

Balasubramanian MK, Bi E, Glotzer M (2004). Comparative analysis of cytokinesis in budding yeast, fission yeast and animal cells. Curr Biol 14, R806–R818.

Balasubramanian MK, McCollum D, Chang L, Wong KC, Naqvi NI, He X, Sazer S, Gould KL (1998). Isolation and characterization of new fission yeast cytokinesis mutants. Genetics 149, 1265–1275.

Basu R, Chang F (2011). Characterization of dip1p reveals a switch in Arp2/3-dependent actin assembly for fission yeast endocytosis. Curr Biol 21, 905–916.

Bathe M, Chang F (2010). Cytokinesis and the contractile ring in fission yeast: towards a systems-level understanding. Trends Microbiol 18, 38–45.

Bezanilla M, Forsburg SL, Pollard TD (1997). Identification of a second myosin-II in Schizosaccharomyces pombe: Myp2p is conditionally required for cytokinesis. Mol Biol Cell 8, 2693–2705.

Bi E, Maddox P, Lew DJ, Salmon ED, McMillan JN, Yeh E, Pringle JR (1998). Involvement of an actomyosin contractile ring in Saccharomyces cerevisiae cytokinesis. J Cell Biol 142, 1301–1312.

Bork P, Sander C, Valencia A (1992). An ATPase domain common to prokaryotic cell cycle proteins, sugar kinases, actin, and hsp70 heat shock proteins. Proc Natl Acad Sci USA 89, 7290–7294.

Calvert ME, Wright GD, Leong FY, Chiam KH, Chen Y, Jedd G, Balasubramanian MK (2011). Myosin concentration underlies cell size-dependent scalability of actomyosin ring constriction. J Cell Biol 195, 799–813.

Carvalho A, Desai A, Oegema K (2009). Structural memory in the contractile ring makes the duration of cytokinesis independent of cell size. Cell 137, 926–937.
Celton-Morizur S, Bordes N, Fraisier V, Tran PT, Paoletti A (2004). C-terminal anchoring of mid1p to membranes stabilizes cytokinetic ring position in early mitosis in fission yeast. Mol Cell Biol 24, 10621–10635.
Chang F (1999). Movement of a cytokinesis factor cdc12p to the site of cell division. Curr Biol 9, 849–852.
Chang F, Drubin D, Nurse P (1997). cdc12p, a protein required for cytokinesis in fission yeast, is a component of the cell division ring and interacts with profilin. J Cell Biol 137, 169–182.
Chang F, Woollard A, Nurse P (1996). Isolation and characterization of fission yeast mutants defective in the assembly and placement of the contractile actin ring. J Cell Sci 109, 131–142.
Cortes JC, Carnero E, Ishiguro J, Sanchez Y, Duran A, Ribas JC (2005). The novel fission yeast (1,3)beta-D-glucan synthase catalytic subunit Bgs4p is essential during both cytokinesis and polarized growth. J Cell Sci 118, 157–174.
Cortes JC, Konomi M, Martins IM, Munoz J, Moreno MB, Osumi M, Duran A, Ribas JC (2007). The (1,3)beta-D-glucan synthase subunit Bgs1p is responsible for the fission yeast primary septum formation. Mol Microbiol 65, 201–217.
Cortes JC, Sato M, Munoz J, Moreno MB, Clemente-Ramos JA, Ramos M, Okada H, Osumi M, Duran A, Ribas JC (2012). Fission yeast Ags1 confers the essential septum strength needed for safe gradual cell abscission. J Cell Biol 198, 637–656.
Dai J, Sheetz MP (1999). Membrane tether formation from blebbing cells. Biophys J 77, 3363–3370.
De Lozanne A, Spudich JA (1987). Disruption of the Dictyostelium myosin heavy chain gene by homologous recombination. Science 236, 1086–1091.
Edelstein A, Amodaj N, Hoover K, Vale R, Stuurman N (2010). Computer control of microscopes using microManager. Curr Protoc Mol Biol Chapter 14, Unit14.20.
Evans E, Yeung A (1989). Apparent viscosity and cortical tension of blood granulocytes determined by micropipet aspiration. Biophys J 56, 151–160.
Fang X, Luo J, Nishihama R, Wloka C, Dravis C, Travaglia M, Iwase M, Vallen EA, Bi E (2010). Biphasic targeting and cleavage furrow ingression directed by the tail of a myosin II. J Cell Biol 191, 1333–1350.
Gould KL, Simanis V (1997). The control of septum formation in fission yeast. Genes Dev 11, 2939–2951.
Gutierrez R, Lindeboom JJ, Paredez AR, Emons AM, Ehrhardt DW (2009). Arabidopsis cortical microtubules position cellulose synthase delivery to the plasma membrane and interact with cellulose synthase trafficking compartments. Nat Cell Biol 11, 797–806.
Hickson GR, O'Farrell PH (2008). Rho-dependent control of anillin behavior during cytokinesis. J Cell Biol 180, 285–294.
Jochova J, Rupes I, Streiblova E (1991). F-actin contractile rings in protoplasts of the yeast Schizosaccharomyces. Cell Biol Int Rep 15, 607–610.
Kamasaki T, Osumi M, Mabuchi I (2007). Three-dimensional arrangement of F-actin in the contractile ring of fission yeast. J Cell Biol 178, 765–771.
Landrein B, Hamant O (2013). How mechanical stress controls microtubule behavior and morphogenesis in plants: history, experiments and revisited theories. Plant J 75, 324–338.
Laplace PS (1805). Supplément au dixième livre du traité de méchanique céleste sur l'action capillaire. Traité de Mécanique Céleste, Paris: Duprat.
Lee WL, Bezanilla M, Pollard TD (2000). Fission yeast myosin-I, Myo1p, stimulates actin assembly by Arp2/3 complex and shares functions with WASp. J Cell Biol 151, 789–800.
Le Goff X, Motegi F, Salimova E, Mabuchi I, Simanis V (2000). The S. pombe rlc1 gene encodes a putative myosin regulatory light chain that binds the type II myosins myo3p and myo2p. J Cell Sci 113, 4157–4163.
Lord M, Laves E, Pollard TD (2005). Cytokinesis depends on the motor domains of myosin-II in fission yeast but not in budding yeast. Mol Biol Cell 16, 5346–5355.
Lutkenhaus J, Pichoff S, Du S (2012). Bacterial cytokinesis: from Z ring to divisome. Cytoskeleton (Hoboken) 69, 778–790.
Ma X, Kovacs M, Conti MA, Wang A, Zhang Y, Sellers JR, Adelstein RS (2012). Nonmuscle myosin II exerts tension but does not translocate actin in vertebrate cytokinesis. Proc Natl Acad Sci USA 109, 4509–4514.
Mandato CA, Bement WM (2001). Contraction and polymerization cooperate to assemble and close actomyosin rings around Xenopus oocyte wounds. J Cell Biol 154, 785–797.
Marks J, Hagan IM, Hyams JS (1987). Spatial association of F-actin with growth polarity and septation in the fission yeast Schizosaccharomyces pombe. Spec Publ Soc Gen Microbiol 23, 119–135.
Mishra M, Kashiwazaki J, Takagi T, Srinivasan R, Huang Y, Balasubramanian MK, Mabuchi I (2013). In vitro contraction of cytokinetic ring depends on myosin II but not on actin dynamics. Nat Cell Biol 15, 853–859.
Mishra M, Karagiannis J, Trautmann S, Wang H, McCollum D, Balasubramanian MK (2004). The Clp1p/Flp1p phosphatase ensures completion of cytokinesis in response to minor perturbation of the cell division machinery in Schizosaccharomyces pombe. J Cell Sci 117, 3897–3910.
Motegi F, Nakano K, Mabuchi I (2000). Molecular mechanism of myosin-II assembly at the division site in Schizosaccharomyces pombe. J Cell Sci 113, 1813–1825.
Naqvi NI, Eng K, Gould KL, Balasubramanian MK (1999). Evidence for F-actin-dependent and -independent mechanisms involved in assembly and stability of the medial actomyosin ring in fission yeast. EMBO J 18, 854–862.
Nurse P, Thuriaux P, Nasmyth K (1976). Genetic control of the cell division cycle in the fission yeast Schizosaccharomyces pombe. Mol Gen Genet 146, 167–178.
Paredez AR, Somerville CR, Ehrhardt DW (2006). Visualization of cellulose synthase demonstrates functional association with microtubules. Science 312, 1491–1495.
Pelham RJ, Chang F (2002). Actin dynamics in the contractile ring during cytokinesis in fission yeast. Nature 419, 82–86.
Pollard LW, Onishi M, Pringle JR, Lord M (2012). Fission yeast Cyk3p is a transglutaminase-like protein that participates in cytokinesis and cell morphogenesis. Mol Biol Cell 23, 2433–2444.
Pollard TD, Wu JQ (2010). Understanding cytokinesis: lessons from fission yeast. Nat Rev Mol Cell Biol 11, 149–155.
Proctor SA, Minc N, Boudaoud A, Chang F (2012). Contributions of turgor pressure, the contractile ring, and septum assembly to forces in cytokinesis in fission yeast. Curr Biol 22, 1601–1608.
Rappaport R (1967). Cell division: direct measurement of maximum tension exerted by furrow of echinoderm eggs. Science 156, 1241–1243.
Roberts-Galbraith RH, Ohi MD, Ballif BA, Chen JS, McLeod I, McDonald WH, Gygi SP, Yates JR 3rd, Gould KL (2010). Dephosphorylation of F-BAR protein Cdc15 modulates its conformation and stimulates its scaffolding activity at the cell division site. Mol Cell 39, 86–99.
Roncero C, Sanchez Y (2010). Cell separation and the maintenance of cell integrity during cytokinesis in yeast: the assembly of a septum. Yeast 27, 521–530.
Schmit AC, Lambert AM (1988). Plant actin filament and microtubule interactions during anaphase–telophase transition: effects of antagonist drugs. Biol Cell 64, 309–319.
Sladewski TE, Previs MJ, Lord M (2009). Regulation of fission yeast myosin-II function and contractile ring dynamics by regulatory light-chain and heavy-chain phosphorylation. Mol Biol Cell 20, 3941–3952.
Smith LG (1999). Divide and conquer: cytokinesis in plant cells. Curr Opin Plant Biol 2, 447–453.
Stachowiak MR, Laplante C, Chin HF, Guirao B, Karatekin E, Pollard TD, O'Shaughnessy B (2014). Mechanism of cytokinetic contractile ring constriction in fission yeast. Dev Cell 29, 547–561.
Tebbs IR, Pollard TD (2013). Separate roles of IQGAP Rng2p in forming and constricting the Schizosaccharomyces pombe cytokinetic contractile ring. Mol Biol Cell 24, 1904–1917.
Thevenaz P, Ruttimann UE, Unser M (1998). A pyramid approach to subpixel registration based on intensity. IEEE Trans Image Processing 7, 27–41.
Thiyagarajan S, Zhou Z, Munteanu L, Chang F, O'Shaughnessy B (2014). The Actomyosin Contractile Ring Regulates Septation during Fission Yeast Cytokinesis. Biophys J 106, 358a.
Turi TG, Webster P, Rose JK (1994). Brefeldin A sensitivity and resistance in Schizosaccharomyces pombe. Isolation of multiple genes conferring resistance. J Biol Chem 269, 24229–24236.
Typas A, Banzhaf M, Gross CA, Vollmer W (2012). From the regulation of peptidoglycan synthesis to bacterial growth and morphology. Nat Rev Microbiol 10, 123–136.

Ursell TS, Nguyen J, Monds RD, Colavin A, Billings G, Ouzounov N, Gitai Z, Shaevitz JW, Huang KC (2014). Rod-like bacterial shape is maintained by feedback between cell curvature and cytoskeletal localization. Proc Natl Acad Sci USA 111, E1025–1034.

Valster AH, Pierson ES, Valenta R, Hepler PK, Emons A (1997). Probing the plant actin cytoskeleton during cytokinesis and interphase by profilin microinjection. Plant Cell 9, 1815–1824.

van Teeffelen S, Wang S, Furchtgott L, Huang KC, Wingreen NS, Shaevitz JW, Gitai Z (2011). The bacterial actin MreB rotates, and rotation depends on cell-wall assembly. Proc Natl Acad Sci USA 108, 15822–15827.

White CL, Gober JW (2012). MreB: pilot or passenger of cell wall synthesis? Trends Microbiol 20, 74–79.

Wu JQ, Kuhn JR, Kovar DR, Pollard TD (2003). Spatial and temporal pathway for assembly and constriction of the contractile ring in fission yeast cytokinesis. Dev Cell 5, 723–734.

Wu JQ, Ye Y, Wang N, Pollard TD, Pringle JR (2010). Cooperation between the septins and the actomyosin ring and role of a cell-integrity pathway during cell division in fission yeast. Genetics 186, 897–915.

Yonetani A, Lustig RJ, Moseley JB, Takeda T, Goode BL, Chang F (2008). Regulation and targeting of the fission yeast formin cdc12p in cytokinesis. Mol Biol Cell 19, 2208–2219.

Zhang W, Robinson DN (2005). Balance of actively generated contractile and resistive forces controls cytokinesis dynamics. Proc Natl Acad Sci USA 102, 7186–7191.